Natural Resources Research, Vol. 32, No. 3, June 2023 (© 2023)
https://doi.org/10.1007/s11053-023-10181-9

Original Paper

Variations in Formation Resistivity and Geometric Tortuosity Factors for Consolidated Niger Delta Formations

Jeffrey Randy Gbonhinbor,[1,5] Zekieni Robert Yelebe,[1,2] Ann Amalate Obuebite,[1] and Augustine Agi[3,4,5]

Received 11 May 2022; accepted 4 March 2023
Published online: 30 March 2023

Formation resistivity evaluation is an essential part of electrical properties measurement of porous media. Such deduced properties are often considered in modeling of associated rock properties for better hydrocarbon exploitation. Cognizance of these properties trend are necessary to ensure acceptable magnitudes for regional-based analyses. The aim of this research study was to establish a trend in formation resistivity factor and geometric tortuosity factor for Niger delta formations in Nigeria. These electrical properties were evaluated via core analysis using direct and alternating current sources. Consolidated core samples were procured from different terrains of producing oilfields in Nigeria. Characterized samples in terms of porosities and permeabilities conformed to existing trends. However, clay minerals embedded in acquired samples resulted in lower values of formation resistivity factor. Deduced formation resistivity factors show acceptable values in the range of 3.55–10.26. Geometric tortuosity factor was adopted to evaluate the tortuous nature of Niger delta porous media due to electrical conductivity. Results obtained for geometric tortuosity factors were all < 1. This was used to infer the highly tortuous and sinuous nature of consolidated Niger delta formations. Furthermore, experimental data were subjected to multivariate regression analysis model of second order. All deduced mathematical formulations were comparatively analyzed with existing geometric tortuosity factor models. Mathematical models show reasonable forecast ability for prescribed porosity range with corrected Akaike's Information Criteria difference of 0.98 and 1.59.

KEY WORDS: Formation resistivity factor, Geometric tortuosity factor, Niger delta, Consolidated formations, Regression analysis.

[1]Department of Petroleum Engineering, Niger Delta University, P. M. B. 071 Wilberforce Island, Bayelsa State, Nigeria.
[2]Department of Chemical Engineering, Niger Delta University, P. M. B. 071 Wilberforce Island, Bayelsa State, Nigeria.
[3]Faculty of Chemical and Process Engineering Technology, College of Engineering Technology, Universiti Malaysia Pahang, 26300 Gambang, Pahang, Malaysia.
[4]Centre for Research in Advanced Fluid and Processes (Fluid Centre), Universiti Malaysia Pahang, 26300 Gambang, Pahang, Malaysia.
[5]To whom correspondence should be addressed; e-mail: gbonhinbor.jeffrey@ndu.edu.ng, augustine@ump.edu.my

INTRODUCTION

Electrical properties of fluid-saturated rocks are often evaluated when drilling for hydrocarbon resources. This formation evaluation stage allows identification of fluid type with respect to its saturation. Their measurements are strongly influenced by fluid found in pore spaces, void orientation/network, and rock type (Bai et al., 2013). Fluid in pore spaces promotes electrical conductivity, while the rock grains transmit no electrical signals. However, clayey formations and hydrocarbons present in voids

are exceptions to electrical conductivity and electrical signal occlusion, respectively. Consequently, the pore's electrical conductivity is made possible due to electrolytic conduction of interstitial water. This formation water contains complex dissolved salts, such as potassium chloride, magnesium chloride, calcium chloride, and sodium chloride (Neff, 2002). The electrical properties examined as a result in this phenomenon have a direct bearing on a formation's resistivity. Resistivity measurements from well logs or experimental investigations may be oriented in relation to formation resistivity factor and geometric tortuosity factor.

Formation resistivity factor relates the resistivity of a completely fluid-saturated formation matrix to the resistivity of fluid present in the void. Generally, formation resistivity factor is known to be above unity with exception to only surface electrical conduction (Ghanbarian et al., 2019). Values of formation resistivity factor less than 1 fail to adequately represent the void features of a formation matrix (Dullien, 1979). Field evaluation of this feature is usually obtained by combining well log data and Archie (1942) empirical formulation. However, most formation resistivity factor via core analysis adapts the modified Archie (1942) model to reflect porosity, Winsauer multiplier, and cementation factor (Winsauer et al., 1952). Parameterization of these properties is often configured to suit the formation matrix of interest (Worthington, 1993). Wyllie and Spangler (1952) also developed a special technique for evaluating formation resistivity factor in the presence of clay minerals. This technique establishes formation resistivity factor from the slope of electrical conductivity of a 100% fluid-saturated porous medium to electrical conductivity of the fluid.

Measurements of conductivity may also be analyzed independently during field investigation by resistivity logs. These logs constitute a suite of wireline electrical logs that quantify the formation's resistivity under in situ conditions. Electrical signals are fed into the formation, while the corresponding electrical resistance of the formation are recorded. Alternatively, in situ electrical signals may be generated by induction principles and its equivalent resistivity inferred from electrical conductivity. These techniques utilize especially configured tools to accomplish resistivity for shallow and deep penetrated measurements. Their operating frequencies facilitate the determination of water saturation, hydrocarbon occupied pore volume, and porosity (Asquith and Krygowski, 2004). However, the accuracy of these resistivity logs is often impaired along wellbore regions consisting of mud filtrate invaded zones. A better representation of a formation's true resistivity may be achieved with the aid of a laterolog, which measures resistivity by propagating electric current into the formation and deducing the potential difference within the wellbore. This logging technique may be considered useful to high conductive water-based drilling muds and a wide range of formations (Misra et al., 2020).

Geometric tortuosity factor is the macroscopic representation in fluid flow via porous media due to reduced concentration gradient when considering the effective pathway. Geometric tortuosity factor is always less than 1 and it can be linked to tortuosity by its reciprocal relation (Hillel, 2004; Abderrahmene et al., 2016). It is often employed to account for the complexity in fluid transportation and characterization of the structural environment in porous beds. By this, theoretical models have been formulated based on pore geometry and topography. These models adequately describe manmade porous beds with distinctive features (Ghanbarian et al., 2019). Empirically deduced geometric tortuosity factors for saturated beds vary between 0.01 and 0.84, while unsaturated beds vary from 0.025 to 0.57 (Shackelford and Daniel, 1991a, 1991b; Bezzar and Ghomari, 2013). These values are often estimated using a direct relationship between formation resistivity factor and tortuosity due to electrical conductivity (Umnova et al., 2005; Promentilla et al., 2009; Lane, 2011). Rhoades and Oster (1986) formulated an analytical relationship for geometric tortuosity factor by electrical conductivity. They demonstrated that geometric tortuosity factor can be derived from the pore volume of cores and gradient of fluid-saturated conductivity against fluid conductivity. This technique also identifies the electrical conductivity due to clay minerals present in the core samples.

Geometric tortuosity factor may be evaluated conceptually from particle image velocimetry, theoretical structural analysis, and empirically adjusted theoretical formulations (Shen and Chen, 2007; Graczyk and Matyka, 2020; Bizhani et al., 2022). Particle image velocimetry is an experimental technique that optically parameterizes fluid flow within an enclosed system. Captured multiple images and subjective dynamic fluid properties are adapted to establish tortuosity of a porous medium. However, resolution limitations and imaging speed applied to

fluid dynamic considerations present challenges in digital rock mechanics (Bizhani et al., 2022). Theoretical structural analysis of porous media is based on adopted physical model representations relative to ideal conditions. Physical model may be represented by stochastic configuration of capillary tubes or confined arrangement of uniform spherical beads. Empirically adjusted theoretical formulations account for unique property variations to suit different conditions. These representations are applied to build tortuosity models for both fluid devoid and occupied pore spaces (Saripalli et al., 2002; Yu and Li, 2004; Yunet al., 2006; Feng and Yu, 2007; Coleman and Vassilicos, 2008; Lanfreyet al., 2010; Li and Yu, 2011). Nonetheless, these models are artificial representations of porous beds that may fail to depict the true tortuosity of a formation.

Permeability evaluation of a conductive porous bed is usually not separated from tests associated with its electrical properties. Field tests by means of resistivity logs are used to appraise permeable formations qualitatively. They provide a comparative resistivity profile for high and low permeable regions in relation to clay deposits. Scientific studies have been ceaseless in ascertaining absolute permeability from electrical resistivity of well logs (e.g., Tong and Tao, 2008; Singh, 2019). Attempts to establish a generic correlation between in situ permeability and electrical resistivity have been marred by inconsistencies (Kirkby et al., 2016; Juandi and Syahril, 2017). Reliance on permeability assessment using routine core analysis (RCA) may be reputed as a common practice. The RCA technique conforms to laboratory single-phase injection of fluid via a core sample under variable or constant head. Permeability reckoning using variable head test requires vertical fluid conveyance through a core sample. Bell (1992) suggested that permeability determination by variable head test is well adapted for low permeable samples below 10 mD.[1] Constant head evaluation of permeability entails the horizontal transportation of single-phase fluid via a formation sample. Low to high permeable core plugs may be adequately captured at reservoir conditions using the constant head test (Gbonhinbor et al., 2021).

Niger delta is an oil rich region in Nigeria that is often examined and characterized for exploitation purpose. Formation resistivity measurements among others constitute part of this assessment process. This assessment allows the quantification of specialized electrical properties such as formation resistivity factor, resistivity index, saturation exponent, tortuosity, and cementation factor. These parameters are configured from well logs and existing correlations with assumptions as prescribed by oilfield operators. Deductions obtained facilitate the determination of water or hydrocarbon saturation for a particular oilfield. Local studies reveal evaluations performed with well log data, existing correlations, and assumed values of relevant variables. Investigations as shown by these studies in Table 1 ignore viable clay minerals in Niger delta formations. These clay minerals control permeability alteration arising from fluid conveyance due to chemical compaction (Anandarajah, 2003; Mondol et al., 2008). In addition, diagenesis initiated by post-sedimentation of formation grains with clayey minerals meliorate formation consolidative features (Jiang, 2012). Niger delta regions are well known to be represented by clayey deposits, coarse grain distribution, barriers, and fault lines (Porrenga, 1966; Oboh, 1992; Odigi, 1994). Negligence to this feature may result in overestimated/underestimated pertinent basic properties of Niger delta formations. Thus, this study attempted to establish a characteristic trend for consolidated formations found within the Niger delta region of Nigeria.

MATERIALS AND METHODS

Materials

Procurement of Core Samples

In total, 16 core samples were each procured from different producing oilfields in the Niger delta region. These samples were classed according their producing terrains as land, swamp, offshore, and deep offshore. Samples acquired from various depths were cut into small cylindrical plugs in line with standard field practice. A Soxhlet extractor was utilized to clean the samples before the attainment of each sample's dehydrated weight. Only consolidated formation samples were subjected to relevant physical evaluations in this study. Tables 2, 3, 4 and 5 summarize some identified physical properties of all procured core samples.

[1] 1 mD = 1 millidarcy = 9.86923×10^{-15} $m^{2.}$

Table 1. Summary of resistivity investigations on Niger delta formations

Authors	Year	Investigation	Gap
Anyiam et al.	2010	Applied well logs and correlations to examine water saturation of a Nigerian green field Assumed formation water resistivity of 0.03, cementation factor in the range of 1.85 to 1.9, and saturation exponent of 1	Evaluation technique did not account for clayey formations Assumed values may overestimate or underestimate water saturation
Oruwori and Ikiensikimama	2010	Considered some oilfield resistivity logs and formulated some correlations Assumed 1.8 as cementation factor and utilized Gen-9 Schlumberger's chart to predict water resistivity	Adopted technique failed to account for possible clay minerals
Agbasi	2013	Deduced water saturation from existing equations and well logs for a Niger delta formation Assumed tortuosity and cementation factor of 1 and 2, respectively	Neglected viable clay formation
Adelu et al.	2016	Examined well log data of an offshore oilfield Study showed mineral present in the formation affected cementation factor	Study lacked the prerequisite evaluation to identify mineral influence
Eze et al.	2016	Reviewed resistivity logs and correlations for water saturation Adopted 0.16 Ωm as water resistivity, 1.9 as saturation exponent, and 1.6 as cementation factor	Assumed values may result in erroneous estimates Inadequate evaluation to eliminate presence of clay minerals
Ogidi et al.	2018	Performed analysis using well log data for an offshore oilfield Assumed saturation exponent of 2	Lack of proper analysis to maximize accuracy

Table 2. Properties of procured core samples for land terrain

Properties	Core sample A1	Core sample A2	Core Sample A3	Core Sample A4
Depth* (ft)	10,927	9,978	9,912	8,831
Length (cm)	7.1	7.2	7.0	6.9
Diameter (cm)	3.72	3.70	3.72	3.70
Dry weight (g)	168.4	169.2	166.3	162.2

*1 ft = 0.3048 m

Table 3. Properties of procured core samples from swamp terrain

Properties	Core sample B1	Core sample B2	Core Sample B3	Core Sample B4
Depth* (ft)	9,800.4	9,720	9,690	9,003
Length (cm)	6.8	7.0	7.1	7.2
Diameter (cm)	3.72	3.71	3.70	3.72
Dry weight (g)	133.55	136.7	138.5	142.0

*1 ft = 0.3048 m

Table 4. Properties of procured core samples from offshore terrain

Properties	Core sample C1	Core sample C2	Core Sample C3	Core Sample C4
Depth* (ft)	10,550	10,450	10,400	10,300
Length (cm)	7.1	6.9	6.8	7.1
Diameter (cm)	3.70	3.70	3.71	3.76
Dry weight (g)	154.09	155.1	155.3	166.6

*1 ft = 0.3048 m

Table 5. Properties of procured core samples from deep offshore terrain

Properties	Core sample D1	Core sample D2	Core Sample D3	Core Sample D4
Depth* (ft)	99,960.4	99,800	99,840	99,732
Length (cm)	6.5	7.1	6.9	7.1
Diameter (cm)	3.77	3.75	3.74	3.71
Dry weight (g)	152.12	163.8	158.3	160.3

*1 ft = 0.3048 m

Preparation of Brine Solution

Salinity concentration levels of 250 ppm, 10,000 ppm, 50,000 ppm, and 95,000 ppm were adapted to evaluate resistivity measurement on core samples. These salinity levels reflect 250 ppm low salinity and 95,000 ppm high salinity conditions for Niger delta formation water (Anyiam et al., 2010; Oruwori and Ikiensikimama, 2010). Sodium chloride (NaCl) was utilized to prepare the salinity formulation through this research. The adopted laboratory salt possesses a 58.44 g/mol molecular weight with 99% assay purity. A summary of brine solution preparation is given in Table 6.

Table 6. Preparation of brine solution

Mass of NaCl (g)	0.25	10	50	95
Volume of water (cm^3)	1000	1000	1000	1000
Concentration of brine (ppm)	250	10,000	50,000	95,000
Viscosity of brine (mPa s)	0.8489	0.8961	1.0140	1.0591

Methods

The properties of all core samples were measured using brine saturation test, steady-state displacement test, and voltage divider technique. These empirical techniques enable determination of porosity, permeability, and resistivity parameters as follows.

Brine Saturation Test

All core samples were placed in a conventional oven and dried intermittently at 40 °C until each sample had a constant dry weight. These samples were transferred to a vacuum chamber containing 1.027 g/cm^3 density of brine. The applied vacuum saturation ensures that all pores were completely liquid-saturated with no air molecule present. Wet weights of various samples were recorded after complete saturation under vacuum conditions. Pore volume, bulk volume, and porosity of each sample were evaluated using formulations identified by Gbonhinbor et al. (2021). The brine saturation test may give an accurate representation of a core sample's porosity in the absence of inaccessible pores (Anovitz and Cole, 2015).

Steady-State Displacement Test

A steady-state displacement test was performed using a displacement experimental setup as shown in Figure 1. This test equipment allows permeability measurement of a core sample by single-phase fluid flow through it at surface conditions. The process equipment is composed of a brine accumulator, connecting pipes, fittings, a displacement pump, a core holder, a U-tube manometer, and a liquid collector. A 250 ppm brine solution was utilized in the displacement test and vacuum saturation of core samples. The 100% brine-saturated core sample was then mounted in the sample holder prior to its fluid displacement. Displacement evaluation commenced by pumping brine solution at a steady flowrate of 0.5 ml/min. The low constant injection rate ensures that laminar flow conditions were satisfied. A differential pressure reading was recorded between the upstream and downstream fittings of the core sample. The experimental procedure was repeated for all core samples and their corresponding absolute permeabilities were evaluated using Darcy's law given by Wyckoff et al. (1933). Strict adherence to Darcy's assumptions may realize permeability measurements at surface conditions similar to in situ conditions.

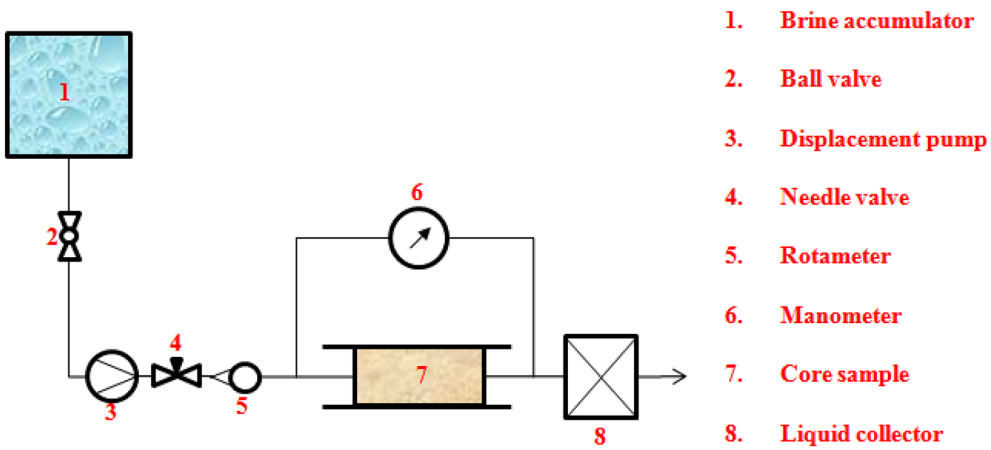

Figure 1. Schematic of single-phase displacement setup.

Voltage Divider Technique

Resistivity parameters of all core samples were determined from the measured resistance of samples using the voltage divider technique. This method measures the resistance of a sample by connecting a reference resistor in series (Fig. 2). The electrical circuits comparatively evaluated resistivity using a low voltage direct current (DC) generator and alternating current (AC) generator. The DC circuit utilized a resistor of 2 Ω, voltmeters, connecting wires, and a switch, while a 4.7 Ω resistor, voltmeters, connecting wires, and a switch were mounted in the AC circuit. Core samples were first saturated with 250 ppm NaCl solution under vacuum conditions. Saturated samples were individually placed in the electrical circuits in order to measure the corresponding voltage drop across it and the reference resistor. Each sample was later washed with distilled water and dried appropriately prior to their corresponding resaturation with 10,000 ppm, 50,000 ppm, and 95,000 ppm NaCl solutions. The resistivity of each core sample was determined from traditional calculations described by Gbonhinbor et al. (2021). Water resistivities at selected salinities were estimated from Schlumberger's resistivity chart for NaCl solutions (Hilchie, 1982). Formation resistivity factor for each sample was ascertained from the slope's reciprocal of brine-saturated sample conductivity against brine conductivity. Ghanbarian et al. (2019) suggested that a low voltage-high frequency AC generator may result in accurate laboratory resistivity assessment.

Statistical Modeling and Validation

Formation resistivity and geometric tortuosity factors were modeled with porosity and clay mineral resistivity in the formation. This allows a general nonlinear multivariate regression model of the second order to be formulated. Data sets generated experimentally were utilized to fit the nonlinear regression model. The analysis was implemented using a specialized algorithm developed by MATLAB™. The algorithm allows a model to be fitted numerically by Gauss–Newton with Levenberg–Marquardt alterations. Estimated coefficients in each model were determined iteratively using initial guesses and a statistical confidence interval of 95%. Nash and Walker–Smith (1987) favors computer algorithm for nonlinear regression analysis due to rigorous process calculations.

Residual error analysis was carried out on the developed models in order to diagnose its reliability in relation to measured responses. This was implemented using well known techniques developed in ordinary residuals by Cox and Snell (1968), Bates and Watts (1980), Clark (1980). These techniques assess residual error by generating vertical lines about each data point and its corresponding model predictor. However, complexity in variable transformation and power series application encourages solution using computers. By this, residual errors were assessed for formation resistivity factor and geometric tortuosity factor. An algorithm developed by MATLAB™ was applied to formulated nonlinear regression at 95% confidence interval. Further validation was carried by

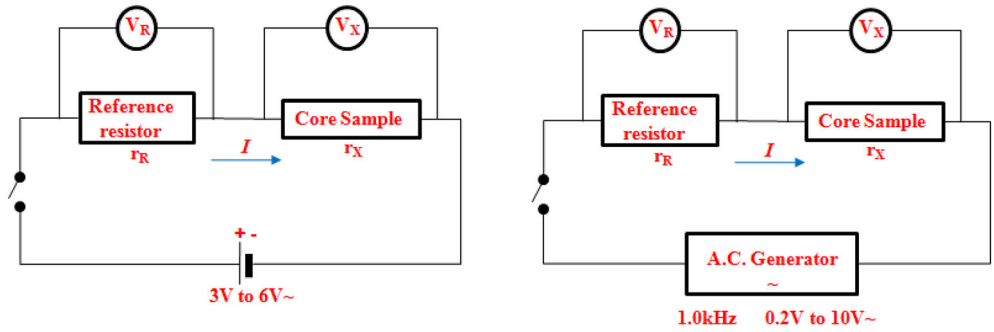

Figure 2. Circuit diagram for resistance measurement.

comparing geometric tortuosity factor with some existing models generated by analytical geometry. These models include Yu and Li (2004), Lanfrey et al. (2010), and Li and Yu (2011). Their selection criterion was based on simplicity as all models were explicit formulations of porosity. Abderrahmene et al. (2016) identified that geometric tortuosity factor may be related to tortuosity by:

$$\tau_m = \frac{1}{\tau} \tag{1}$$

where τ_m is geometric tortuosity factor and τ is tortuosity. Thus, the geometric tortuosity model of Yu and Li (2004) becomes:

$$\tau_m|_{sat} = \left[\frac{1}{2}\left[1 + \frac{1}{2}\sqrt{1-\phi} + \frac{\sqrt{(1-\sqrt{1-\phi})^2 + \frac{1-\phi}{4}}}{1-\sqrt{1-\phi}}\right]\right]^{-1} \tag{2}$$

where $\tau_m|_{sat}$ is geometric tortuosity factor for a saturated porous medium. The geometric tortuosity model of Lanfrey et al. (2010) may be expressed as:

$$\tau_m|_{sat} = \left[1.23\frac{(1-\phi)^{\frac{4}{3}}}{\xi^2\phi}\right]^{-1} \tag{3}$$

where ξ is a round factor. Lanfrey et al. (2010) suggested that this factor is equal to 1 for spherical grains and less than 1 for non-spherical grains. The geometric tortuosity factor of Li and Yu (2011) may be represented as:

$$\tau_m|_{sat} = \left[\left(\frac{19}{18}\right)^{\frac{\ln(\phi)}{\ln\left(\frac{8}{9}\right)}}\right]^{-1} \tag{4}$$

RESULTS AND DISCUSSION

A minimum porosity of 6.2% and a maximum porosity of 17.6% were obtained for all analyzed core samples. These core porosities reflect the true in situ porosities of the reservoirs at various depths due to their respective consolidation. Their observed physical appearances make them insusceptible to prevailing reservoir overburden pressures. Thus, the core porosities were accurately established from known laboratory fluid saturation density. These observed porosities are in line with core samples analyzed by Chiamogu and Ehinola (2010). Their core analyses showed a low porosity of 3.6% at progressive depths in Niger delta regions. Similarly, Ikeagwuani (1979) recorded a porosity of 15% at a depth of 15,000 ft[2] from well log data in a Niger delta oilfield. Permeability values ranging from 1340.1 to 9652.8 mD were computed for all analyzed core samples. These very high permeabilities reflect known excellent permeabilities of all consolidated and unconsolidated Niger delta formations. These results fall within the accepted permeabilities reported by several authors (e.g., Ekine and Iyabe, 2009; Odoh et al., 2012; Nwosu and Ndubueze, 2016; Alaminiokuma and Ofuyah, 2017; Anyiam et al., 2017; Ehigiator and Chigbata, 2017; Inyang et al., 2017; Ogidiet al., 2018; Orji et al., 2019). Tables 7, 8, 9 and 10 list the porosity and permeability of each core sample.

[2] * 1 ft = 0.3048 m.

Table 7. Porosity and permeability of core samples from land terrain

Properties	Core sample A1	Core sample A2	Core sample A3	Core Sample A4
ϕ (%)	12.0	13.5	13.8	14.9
k (md)	1,404.3	1,398.4	1,384.5	1,340.1

Table 8. Porosity and permeability of core samples from swamp terrain

Properties	Core sample B1	Core sample B2	Core sample B3	Core Sample B4
ϕ (%)	17.6	14.8	16.5	15.6
k (md)	1,633.2	1,820.3	1,787.5	1,669.6

Table 9. Porosity and permeability of core samples from offshore terrain

Properties	Core sample C1	Core sample C2	Core sample C3	Core Sample C4
ϕ (%)	6.2	6.7	9.0	10.7
k (md)	9,652.8	7,817.4	5,108.4	4,673.6

Table 10. Porosity and permeability of core samples from deep offshore terrain

Properties	Core sample D1	Core sample D2	Core sample D3	Core Sample D4
ϕ (%)	9.9	10.6	10.9	11.3
k (md)	2,837.3	3,356.1	2,869.1	3,000.2

Electrical resistances of 0.76 to 1525.93 Ω were computed for all core samples at different salinities. These values yielded different core resistivities of 0.013 to 24.259 Ωm under various 100% brine saturation. The DC source was responsible for very low core resistivities, while the AC yielded a low resistivity of 0.26 Ωm. Well logs in Niger delta formations have recorded 0.03–6.98 Ωm at different saturations (Anyiam et al., 2010; Eze et al., 2016; Ogidi et al., 2018). Resistivity measurements using a low voltage AC source was in line Niger delta well logs. The obtained experimental resistivity may infer the presence of conductive solids. However, this inference can only be ascertained by a graphical relationship between saturated rock conductivity and water conductivity. Tables 11, 12, 13, 14, 15, 16, 17 and 18 provide DC and AC electrical resistivity data for all core samples. Figures 3 and 4 provide the rock-saturated conductivity against brine conductivity for both sources.

Figure 3 yielded formation resistivity factors ranging from 0.33 to 0.73 for all core samples. These values infer only surface electrical conduction due to all deduced formation resistivity factors below 1 (Ghanbarian et al., 2019). Ghanbarian et al. (2019) identified that formation resistivity factor cannot be less than 1 based on acceptable definitions. Figure 4 resulted in low formation resistivity factors of 3.55 to 10.26 for all analyzed samples. All experimentally deduced rock-saturated conductivity values were analogous to the range of values obtained by Abderrahmene et al. (2016). These values were most likely influenced by the rock matrix type and clay minerals present. However, formation resistivity factors greater than 1 suggest that electrical conductivity traveled through the porous media (Ghanbarian et al., 2019). Dullien (1979) suggested that pore geometry plays a crucial role in formation resistivity factors above 1. Moreover, further analyses showed resistivity due to clay minerals ranging from 0.96 to 9.65 Ωm. Niger delta formations are

Table 11. DC resistivity data of core samples from land terrain

Properties	Core sample A1				Core sample A2			
Salinity (ppm)	250	10,000	50,000	95,000	250	10,000	50,000	95,000
r_x (Ω)	1.51	1.35	1.17	0.96	1.53	1.30	1.14	0.94
R_{oa} (Ωm)	0.023	0.021	0.018	0.015	0.023	0.019	0.017	0.014
Properties	Core sample A3				Core sample A4			
Salinity (ppm)	250	10,000	50,000	95,000	250	10,000	50,000	95,000
r_x (Ω)	1.47	1.37	1.12	0.94	1.47	1.32	1.09	0.93
R_{oa} (Ωm)	0.023	0.021	0.017	0.015	0.023	0.021	0.017	0.014

Table 12. DC resistivity data of core samples from swamp terrain

Properties	Core sample B1				Core sample B2			
Salinity (ppm)	250	10,000	50,000	95,000	250	10,000	50,000	95,000
r_x (Ω)	1.23	1.12	1.05	0.87	1.26	1.09	1.02	0.87
R_{oa} (Ωm)	0.020	0.018	0.017	0.014	0.020	0.017	0.016	0.013
Properties	Core sample B3				Core sample B4			
Salinity (ppm)	250	10,000	50,000	95,000	250	10,000	50,000	95,000
r_x (Ω)	1.20	1.14	1.00	0.89	1.19	1.10	1.01	0.91
R_{oa} (Ωm)	0.018	0.017	0.015	0.013	0.018	0.017	0.015	0.014

Table 13. DC resistivity data of core samples from offshore terrain

Properties	Core sample C1				Core sample C2			
Salinity (ppm)	250	10,000	50,000	95,000	250	10,000	50,000	95,000
r_x (Ω)	1.42	1.10	0.91	0.78	1.46	1.11	0.92	0.78
R_{oa} (Ωm)	0.022	0.017	0.014	0.012	0.023	0.017	0.014	0.012
Properties	Core sample C3				Core sample C4			
Salinity (ppm)	250	10,000	50,000	95,000	250	10,000	50,000	95,000
r_x (Ω)	1.38	1.07	0.91	0.76	1.36	1.06	0.87	0.75
R_{oa} (Ωm)	0.022	0.017	0.015	0.012	0.021	0.017	0.014	0.012

known to contain clay minerals such as kaolinite, illite, and illite–smectite (Porrenga, 1966; Oboh, 1992; Odigi, 1994). Consequently, geometric tortuosity factors of 0.01 to 0.03 were derived for all core samples due to their respective AC electrical conductivity. These values are within the known empirically derived geometric tortuosity factors of 0.01 to 0.84 in saturated porous media (Shackelford and Daniel, 1991a, 1991b; Bezzar and Ghomari, 2013; Abderrahmene et al., 2016). The obtained geometry tortuosity factors are consistent with low porosity, highly sinuous and tortuous clayey consolidated samples. Tables 19, 20, 21 and 22 illustrate all derived formation resistivity factors, clayey

Table 14. DC resistivity data of core samples from deep offshore terrain

Properties	Core sample D1				Core sample D2			
Salinity (ppm)	250	10,000	50,000	95,000	250	10,000	50,000	95,000
r_x (Ω)	1.17	1.05	0.87	0.76	1.20	1.07	0.91	0.80
R_{oa} (Ωm)	0.020	0.018	0.015	0.013	0.019	0.017	0.014	0.012
Properties	Core sample D3				Core sample D4			
Salinity (ppm)	250	10,000	50,000	95,000	250	10,000	50,000	95,000
r_x (Ω)	1.14	1.02	0.86	0.75	1.12	1.01	0.87	0.76
R_{oa} (Ωm)	0.018	0.016	0.014	0.012	0.017	0.015	0.013	0.012

Table 15. AC resistivity data of core samples from land terrain

Properties	Core sample A1				Core sample A2			
Salinity (ppm)	250	10,000	50,000	95,000	250	10,000	50,000	95,000
r_x (Ω)	96.53	229.87	52.13	18.94	93.30	293.92	51.07	19.13
R_{oa} (Ωm)	1.478	3.519	0.798	0.290	1.393	3.583	0.763	0.286
Properties	Core sample A3				Core sample A4			
Salinity (ppm)	250	10,000	50,000	95,000	250	10,000	50,000	95,000
r_x (Ω)	100.02	220.49	53.18	18.72	90.31	201.16	50.07	18.62
R_{oa} (Ωm)	1.553	3.423	0.826	0.291	1.407	3.135	0.780	0.290

Table 16. AC resistivity data of core samples from swamp terrain

Properties	Core sample B1				Core sample B2			
Salinity (ppm)	250	10,000	50,000	95,000	250	10,000	50,000	95,000
r_x (Ω)	143.94	38.58	17.32	17.59	140.00	38.80	17.22	17.87
R_{oa} (Ωm)	2.301	0.617	0.277	0.281	2.162	0.599	0.266	0.276
Properties	Core sample B3				Core sample B4			
Salinity (ppm)	250	10,000	50,000	95,000	250	10,000	50,000	95,000
r_x (Ω)	148.13	38.33	17.49	17.39	132.27	37.09	17.20	17.42
R_{oa} (Ωm)	2.243	0.580	0.265	0.263	1.997	0.560	0.260	0.263

resistivity present, and tortuosity factors for all analyzed core samples.

The experimental results for only AC formation resistivity factor and geometric tortuosity factor were modeled directly by regression analysis. This is evident as some theoretical formation resistivity factor and tortuosity models are usually expressed as a function of porosity (Yu and Li, 2004; Lanfrey et al., 2010; Li and Yu, 2011). However, clay minerals in the formation were accounted for by introducing a 'clay mineral term' in the regression model. The applied regression technique yielded Eqs. 5 and 6 for formation resistivity factor and geometric tor-

Table 17. AC resistivity data of core samples from offshore terrain

Properties	Core sample C1				Core sample C2			
Salinity (ppm)	250	10,000	50,000	95,000	250	10,000	50,000	95,000
r_x (Ω)	1146.80	200.78	41.47	36.43	919.32	208.37	40.79	37.24
R_{oa} (Ωm)	17.367	3.041	0.628	0.552	14.326	3.247	0.636	0.580
Properties	Core sample C3				Core sample C4			
Salinity (ppm)	250	10,000	50,000	95,000	250	10,000	50,000	95,000
r_x (Ω)	1525.93	193.60	42.12	35.46	767.67	178.26	40.14	35.01
R_{oa} (Ωm)	24.259	3.078	0.670	0.564	12.005	2.788	0.628	0.548

Table 18. AC resistivity data of core samples from deep offshore terrain

Properties	Core sample D1				Core sample D2			
Salinity (ppm)	250	10,000	50,000	95,000	250	10,000	50,000	95,000
r_x (Ω)	169.20	189.45	42.07	44.96	159.21	196.65	41.37	46.84
R_{oa} (Ωm)	2.906	3.253	0.723	0.772	2.477	3.059	0.644	0.729
Properties	Core sample D3				Core sample D4			
Salinity (ppm)	250	10,000	50,000	95,000	250	10,000	50,000	95,000
r_x (Ω)	174.57	182.95	42.76	43.33	150.40	168.88	40.69	42.59
R_{oa} (Ωm)	2.779	2.913	0.681	0.690	2.290	2.571	0.620	0.648

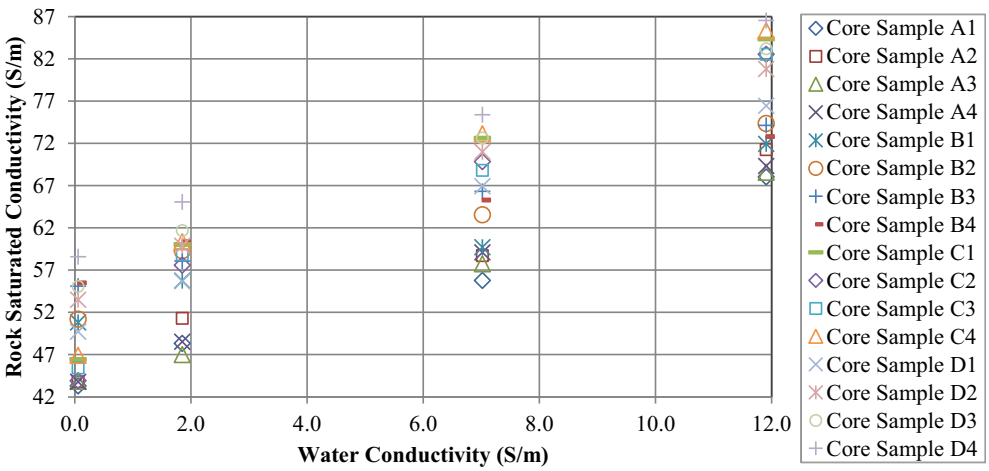

Figure 3. Rock–fluid DC-saturated conductivity of all core samples.

tuosity factor, respectively. Their deduced coefficients are given in Tables 23 and 24.

$$F = A_0 + A_1\phi + A_2R_c + A_3\phi R_c + A_4R_c^2 \quad (5)$$

$$\tau_m = B_0 + B_1\phi + B_2R_c + B_3\phi R_c + B_4\phi^2 + B_5R_c^2 \quad (6)$$

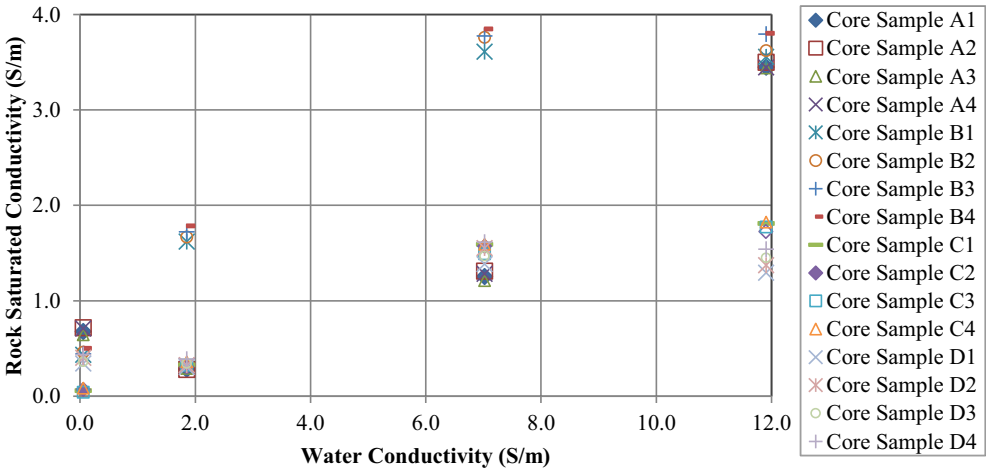

Figure 4. Rock–fluid DC-saturated conductivity of all core samples.

Table 19. Derived electrical properties for all samples from land terrain

Properties	Core samples			
	A1	A2	A3	A4
DC: F	0.50	0.46	0.48	0.47
AC: F	4.11	4.06	4.10	4.16
R_c (Ωm)	6.77	5.94	7.79	5.35
τ_m	0.03	0.02	0.02	0.02

Table 20. Derived electrical properties for all samples from swamp terrain

Properties	Core samples			
	B1	B2	B3	B4
DC: F	0.61	0.57	0.62	0.73
AC: F	3.79	3.72	3.55	3.60
R_c (Ωm)	1.07	1.02	1.03	0.96
τ_m	0.02	0.02	0.02	0.02

Table 21. Derived electrical properties for all samples from offshore terrain

Properties	Core samples			
	C1	C2	C3	C4
DC: F	0.34	0.33	0.35	0.33
AC: F	6.31	6.61	6.47	6.37
R_c (Ωm)	8.16	7.63	9.65	6.74
τ_m	0.03	0.03	0.02	0.02

Table 22. Derived electrical properties for all samples from deep offshore terrain

Properties	Core samples			
	D1	D2	D3	D4
DC: F	0.45	0.44	0.43	0.44
AC: F	10.26	9.74	9.18	8.86
R_c (Ωm)	3.08	2.64	2.96	2.45
τ_m	0.01	0.01	0.01	0.01

Both models (Eqs. 5 and 6) were validated with their respective experimental data. Niger delta formation resistivity factors for consolidated and unconsolidated formations are commonly estimated with Archie (1942) equation (Oruwori and Ikiensikimama, 2010; Agbasi, 2013; Eze et al., 2016). This is usually achieved by selecting a cementation factor value and sometimes Winsauer constant. Conductivity due to clay minerals renders the Archie (1942) equation unfit for estimation. Thus, on the one hand, only Eq. 5 is compared with its corresponding experimental outcomes. On the other hand, Eq. 6 is compared with known aforementioned geometric tortuosity factor models. The corrected Akaike's Information Criteria (AIC) difference between experimental data relative to Eqs. 5 and 6 are 0.98 and 1.59, respectively. The geometric tortuosity model of Lanfrey et al. (2010) yielded corrected AIC difference of 3.64 relative to assumed roundness factors below 1. Similarly, AIC differences of 60.61

Table 23. Derived coefficients for formation resistivity factor model

Variable	Definition	Magnitude
A_0	Dimensionless formation factor constant	2.8520×10^{1}
A_1	Dimensionless porosity coefficient in formation factor	-1.4808×10^{2}
A_2	Resistivity coefficient in formation factor, $\Omega^{-1}m^{-1}$	-3.0923×10^{0}
A_3	Porosity–resistivity coefficient in formation factor, $\Omega^{-1}m^{-1}$	1.4380×10^{1}
A_4	Squared resistivity coefficient in formation factor, $\Omega^{-2}m^{-2}$	8.1412×10^{-2}

Table 24. Derived coefficients for geometric tortuosity factor model

Variable	Definition	Magnitude
B_0	Dimensionless geometric tortuosity constant	-8.2472×10^{-2}
B_1	Dimensionless porosity coefficient in geometric tortuosity factor	8.1888×10^{-1}
B_2	Resistivity coefficient in geometric tortuosity factor, $\Omega^{-1}m^{-1}$	1.9121×10^{-2}
B_3	Porosity–resistivity coefficient in geometric tortuosity factor, $\Omega^{-1}m^{-1}$	-8.9128×10^{-2}
B_4	Squared dimensionless porosity coefficient in geometric tortuosity factor	-1.3229×10^{0}
B_5	Squared resistivity coefficient in geometric tortuosity factor, $\Omega^{-2}m^{-2}$	-6.7972×10^{-4}

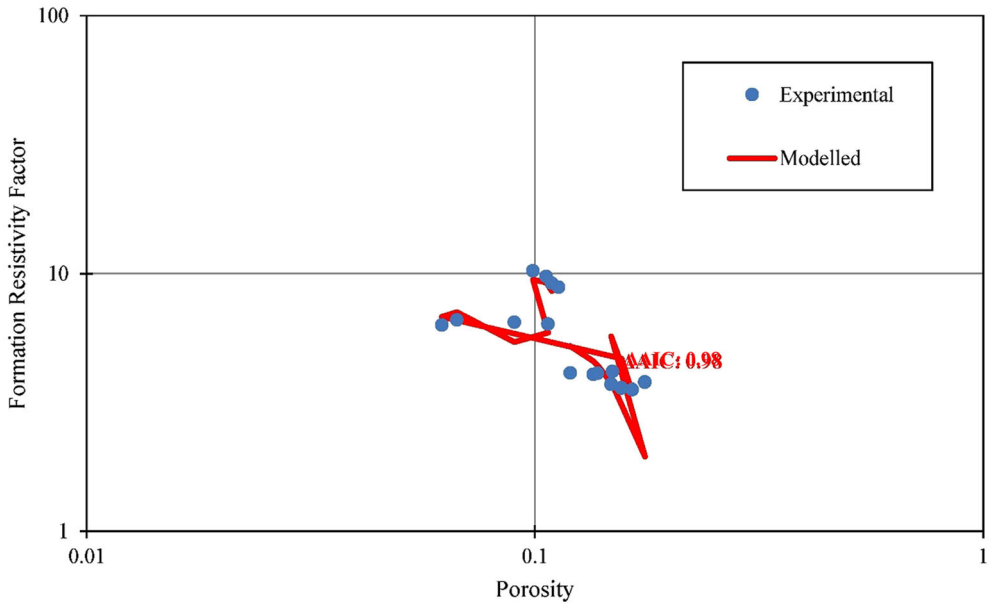

Figure 5. Comparison of experimental and modeled formation resistivity factor.

and 57.30 were incurred for both models of Yu and Li (2004) and Li and Yu (2011). These data suggest inadequate predictability of the geometric tortuosity factor models of Yu and Li (2004) and Li and Yu (2011). Comparison of experimental data with model predicted data are shown in Figures 5 and 6.

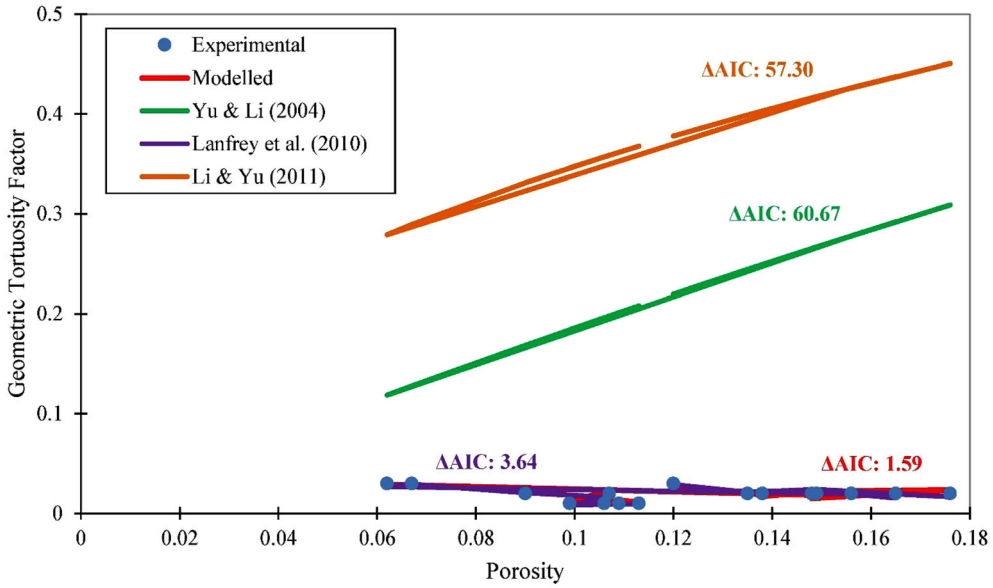

Figure 6. Comparison of experimental and modeled geometric tortuosity factors.

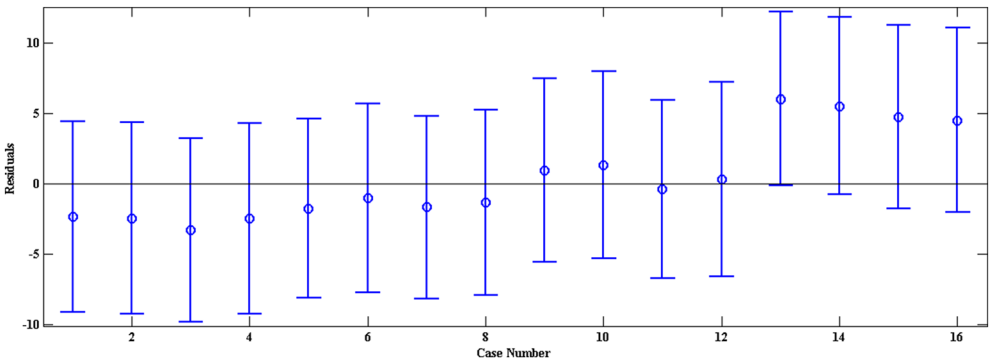

Figure 7. Residual case order plot for formation resistivity factor model.

Figure 7 shows the goodness of fit for all data points in the residual order case plot associated with Eq. 5. This analysis suggests that the experimental data were within the upper and lower bounds of the formation resistivity factor model. The residual order case performance of Figure 8 in relation to Eq. 6 is analogous to Figure 7. This trend confirmed an unbiased and established formation resistivity and geometric tortuosity factor models. Therefore, the attained coefficients may facilitate adequate predictions of dependent variables in both models.

CONCLUSIONS

The study approach applied in this research indicated the following.

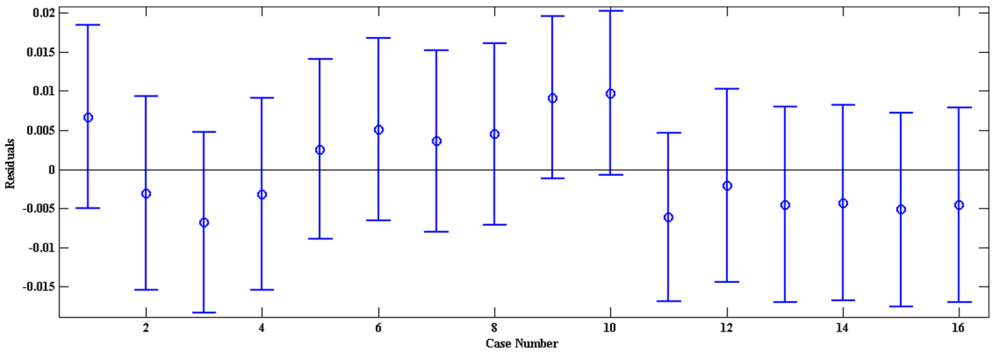

Figure 8. Residual order case plot for geometric tortuosity factor model.

All analyzed consolidated core samples were characterized by low porosities match with very high permeabilities. Minimum and maximum porosity differences of 0.1% and 12.4% were observed among all samples. Conversely, permeability differences of 8,312.7 and 44.4 mD were recorded among sample terrains. Generally, these core samples showed a fair inverse variational relationship in the porosity–permeability data. Proper liquid saturation of these cores could only be achieved in the laboratory by vacuum saturation condition. This feature is mostly likely to be controlled by the samples' degree of compactness and cementation.

Low formation resistivity factors were established for all core samples analyzed in this study. However, the formation resistivity factors obtained from DC source were rejected due unsatisfactory performance. A maximum difference of 6.71 was matched by a minimum difference of 0.01 between core samples subject to AC source. The low formation resistivity factors were a result of solid and electrolyte conduction in the examined samples. The abundance of clay minerals in the samples could not be ascertained from the applied conductivity technique. These values were below the known estimated techniques from other local authors. Local authors assumed zero solid conduction, which is likely erroneous when examining most Niger delta formations. Clay minerals present affected the determination of tortuosity by replacing it with a geometric tortuosity factor. This geometric tortuosity factor of each sample showed minimal difference in variation of samples. Nonetheless, all analyzed sample data infer very tortuous and sinuous geometry of flow path.

Both developed models draw good empirical correlations among porosity, clay mineral conductivity, formation resistivity, and geometric tortuosity factors. Computed minimal deviations enhance the usefulness of these simple and concise models. Assumed values of roundness factor from the Lanfrey et al. (2010) model is a limitation to forecast geometric tortuosity factor without experimental data. Residual error analyses showed good fit of developed models favoring assumptions inherent in the regression technique. By this, established coefficients were estimated with favorable certainty. Consequently, the developed models are likely to forecast formation resistivity or geometric tortuosity factors for consolidated clayey formations in Niger delta.

ACKNOWLEDGMENTS

Authors would like to acknowledge Mr. Kalu Obasi Onuma of Ansett Integrated Services Limited in Port Harcourt, Nigeria. He played an invaluable role in the acquisition and treatment of all core samples utilized in this research work.

DECLARATIONS

Conflict of Interest All authors of this research did not receive funding or support from any organization. We declare no completing interests germane to the information provided in this work.

REFERENCES

Abderrahmene, M., Abdelillah, B., & Fouad, G. (2016). Electrical prediction of tortuosity in porous media. In *Proceeding at the*

international conference on materials and energy, La Rochelle, France. https://doi.org/10.1016/j.egypro.2017.11.277.
Adelu, A. O., Sanuade, O. A., Oboh, E. G., Offeh, E. O., Adewale, T., Mumuni, O. S., Oladapo, I. M., & Omolaiye, E. G. (2016). Hydrocarbon field evaluation: Case study of 'Tadelu' field shallow offshore Western Niger Delta, Nigeria. *Arabian Journal of Geosciences, 9*(2), 303–330.
Agbasi, O. E. (2013). Estimation of water saturation using a modeled equation and Archie's equation from wire-line logs, Niger Delta Nigeria. *Journal of Applied Physics, 3*(4), 66–71.
Alaminiokuma, G. I., & Ofuyah, W. N. (2017). Porosity-permeability regimes in reservoirs for hydrocarbon prospectivity in Nembe creek field, Niger Delta. *Journal of Applied Geology and Geophysics, 5*(2), 62–70.
Anandarajah, A. (2003). Mechanism controlling permeability change in clays due to change in pore fluid. *Journal of Geotechnical and Geoenvironmental Engineering, 129*(2), 163–172.
Anovitz, L. M., & Cole, D. R. (2015). Characterization and analysis of porosity and pore structures. *Reviews in Mineralogy and Geochemistry, 80*(1), 61–164.
Anyiam, O. A., Andrew, P. J., & Okwara, I. C. (2017). Assessment of the heterogeneity and petrophysical evaluation of reservoirs in the ''Akbar Field'', Niger Delta, Nigeria. *Journal of Petroleum Exploration and Production Technology, 7*(4), 1033–1050.
Anyiam, O. A., Mode, A. W., & Ekwe, A. C. (2010). Formation evaluation of an onshore appraisal well 'KG-5', ''Green Field'', Niger Delta, Nigeria. *American Journal of Scientific and Industrial Research, 1*(2), 262–270.
Archie, G. E. (1942). The electrical resistivity log as an aid in determining some reservoir characteristics. *Transactions of the AIME, 146*(1), 54–63. SPE-942054-G.
Asquith, G., & Krygowski, D. (2004). *Basic well log analysis* (2nd ed.). AAPG.
Bai, W., Kong, L., & Guo, A. (2013). Effects of physical properties on electrical conductivity of compacted lateritic soil. *Journal of Rock Mechanics and Geotechnical Engineering, 5*(5), 406–411.
Bates, D. M., & Watts, D. G. (1980). Relative curvature measures of nonlinearity. *Journal of Royal Statistical Society. Series B (Methodological), 42*(1), 1–25.
Bell, F. G. (1992). *Engineering properties of soils and rocks* (3rd ed.). Butterworth Heinemann.
Bezzar, A., & Ghomari, F. (2013). Montoring of pollutant diffusion into clay liners by electrical methods. *Transport in Porous Media, 97*(2), 147–159.
Bizhani, M., Ardakani, O. H., & Little, E. (2022). Reconstructing high fidelity digital rock images using deep convolutional neutral networks. *Scientific Reports, 12*, 4264.
Chiamogu, G.A., & Ehinola, O.A. (2010). Distribution patterns of porosity and permeability in the hydrocarbon bearing sands of Agbada formation, Niger Delta continental shelf, Nigeria. *Presented at the AAPG International Convention and Exhibition*, Calgary, Canada.
Clark, G. P. Y. (1980). Moments of the least squares estimators in non-linear regression model. *Journal of Royal Statistical Society. Series B (Methodological), 42*(2), 227–237.
Coleman, S. W., & Vassilicos, J. C. (2008). Transport properties of saturated and unsaturated porous fractal materials. *Physical Review Letters, 100*(3), 035504.
Cox, D. R., & Snell, E. J. (1968). A general definition of residuals. *Journal of Royal Statistical Society. Series B (Methodological), 30*(2), 248–275.
Dullien, F. A. L. (1979). *Porous media: Fluid transport and pore structure*. Academic Press.
Ehigiator, M. O., & Chigbata, N. C. (2017). Geophysical and well correlation analysis of Ogo Field: A case study in Niger Delta Basin of Nigeria. *Nigerian Journal of Technology, 36*(3), 729–733.
Ekine, A. S., & Iyabe, P. (2009). Petrophysical Characterization of the Kwale Field reservoir sands (OML 60) from wire-line logs, Niger Delta, Nigeria. *Journal of Applied Sciences and Environmental Management, 13*(4), 81–85.
Eze, M. O., Mode, A. W., & Anyiam, A. O. (2016). Recognition and evaluation of low resistivity pay-zones: A case study of ''Amo-Field'' in tertiary Niger Delta Basin, Nigeria. *The Pacific Journal of Science and Technology, 17*(1), 337–344.
Feng, Y., & Yu, B. (2007). Fractal dimension for tortuous stream tubes in porous media. *Fractals, 15*(4), 385–390.
Gbonhinbor, J. R., Igbani, S., & Yelebe, Z. R. (2021). *Practical manual on petroleum engineering laboratory II (PEE 332)*. Kadmon Printing Company Limited.
Ghanbarian, B., Lake, L. W., & Sahimi, M. (2019). Insights into rock typing: A critical study. *SPE Journal, 24*(1), 230–242. https://doi.org/10.2118/191366-PA. SPE-191366-PA.
Graczyk, K. M., & Matyka, M. (2020). Predicting porosity, permeability, and tortuosity of porous media from images by deep learning. *Scientific Reports, 10*, 21488.
Hilchie, D.W. (1982). *Applied Openhole log interpretation for geologists and engineers (Revised Ed.)*. Douglas W. Hilchie Inc., Golden, CO.
Hillel, D. (2004). *Introduction to environmental soil physics*. Academic Press.
Ikeagwuani, F. O. (1979). *Trends of petroleum exploration in Nigeria*. Nigerian National Petroleum Corporation Report.
Inyang, N. J., Akpabio, I. O., & Agbasi, O. E. (2017). Shale volume and permeability of the Miocene unconsolidated Turbidite sands of Bonga Oil field, Niger Delta, Nigeria. *International Journal of Advanced Geosciences, 5*(1), 37–45.
Jiang, S. (2012). Clay minerals from the perspective of oil and gas exploration. In M. Valaškova & G. S. Martynkova (Eds.), *Clay minerals in nature—Their characterization modification and application* (pp. 21–38). IntechOpen.
Juandi, M., & Syahril, S. (2017). Empirical relationship between soil permeability and resistivity, and its application for determining the groundwater gross recharge in Marpoyan Damai, Pekanbaru, Indonesia. *Water Practice and Technology, 12*(3), 660–666.
Kirkby, A., Heinson, G., & Krieger, L. (2016). Relating electrical resistivity to permeability using resistor networks. In *Proceedings at ASEG-PESA-AIG 25th geophysical conference and exhibition*, Adelaide, Australia. https://doi.org/10.1071/ASEG2016ab259.
Lane, N. M. (2011). *Numerical studies of flow in porous media using an unstructured approach*. Doctoral Dissertation LSU.
Lanfrey, P.-Y., Kuzeljevic, Z. V., & Dudukovic, M. P. (2010). Tortuosity model for fixed beds randomly packed with identical particles. *Chemical Engineering Science, 65*(5), 1891–1896.
Li, J.-H., & Yu, B.-M. (2011). Tortuosity of flow paths through a Sierpinski Carpet. *Chinese Physics Letter, 28*(3), 1741–1745.
Misra, S., Tathed, P., & Han, Y. (2020). Characterization of subsurface hydrocarbon/water saturation by processing subsurface electromagnetic logs using a modified Levenberg-Marquardt algorithm. In S. Misra, H. Li, & J. He (Eds.), *Machine learning for subsurface characterization* (pp. 339–368). Gulf Professional Publishing.
Mondol, N. H., Bjørlykke, K., & Jahren, J. (2008). Experimental compaction of clays: Relationship between permeability and petrophysical properties in mudstones. *Petroleum Geoscience, 14*(4), 319–337.
Nash, J., & Walker-Smith, M. (1987). *Nonlinear parameter estimation: An integrated system in BASIC*. Marcel Dekker Inc.
Neff, J. M. (2002). *Bioaccumulation in Marine organisms: Effect of contaminants from oil well produced water*. Elsevier Science.

Nwosu, L. I., & Ndubueze, D. N. (2016). Formation evaluation of an Onshore Oil field, Niger Delta Nigeria. *Journal of Applied Geology and Geophysics, 4*(6), 36–47.

Oboh, F. E. (1992). Middle Miocene palaeoenvironments of the Niger Delta. *Palaeography, Palaeoclimatology, Palaeoecology, 92*(1–2), 55–84.

Odigi, M. I. (1994). Clay-mineral studies of the subsurface Niger Delta. *Journal of Petroleum Geology, 17*(4), 445–460.

Odoh, B. I., Onyeji, J., & Utom, A. U. (2012). The integrated seismic reservoir characterization (ISRC), study in Amboy field of Niger Delta oil field—Nigeria. *Geosciences, 2*(3), 60–65.

Ogidi, A. O., Ekhalialu, O. M., & Okon, E. E. (2018). Petrophysical evaluation of Otebe field, Onshore Niger Delta, Nigeria. *International Journal of Research and Innovation in Applied Science, 3*(11), 2454–6194.

Orji, C. S., Uko, E. D., & Tamunobereton-ari, I. (2019). Permeability-porosity trends in CAWC reservoir sands in the Niger delta Nigeria, using well-log data. *Malaysian Journal of Geosciences, 3*(2), 33–42.

Oruwori, A.E., & Ikiensikimama, S.S. (2010). Determination of water salinities in hydrocarbon bearing reservoirs of some Niger delta fields—Nigeria. In *Proceedings at the SPE Nigeria annual international conference and exhibition*, Calabar, Nigeria. SPE-136997-MS.

Porrenga, H. D. (1966). *Clay mineral in recent sediments of the Niger delta*. Pergamon Press.

Promentilla, M. A. B., Sugiyama, T., Hitomi, T., & Takeda, N. (2009). Quantification of tortuosity in hardened cement pastes using synchrotron-based X-ray computed microtomography. *Cement and Concrete Research, 39*(6), 548–557.

Rhoades, J. D., & Oster, J. D. (1986). *Solute content—Methods of soil analysis part 1: Physical and mineralogical methods* (2nd ed.). American Society of Agronomy – Soil Science Society of America.

Saripalli, K. P., Serne, R. J., Meyer, P. D., & McGrail, B. P. (2002). Prediction of diffusion coefficients in porous media using tortuosity factors based on interfacial areas. *Groundwater, 40*(4), 346–352.

Shackelford, C. D., & Daniel, D. E. (1991a). Diffusion in saturated soil I: Background. *Journal of Geotechnical Engineering, 117*(3), 467–484.

Shackelford, C. D., & Daniel, D. E. (1991b). Diffusion in saturated soil II: Results of compacted clay. *Journal of Geotechnical Engineering, 117*(3), 485–506.

Shen, L., & Chen, Z. (2007). Critical review of the impact of tortuosity on diffusion. *Chemical Engineering Science, 62*(14), 3748–3755.

Singh, N. P. (2019). Permeability prediction from wireline logging and core data: A case study from Assam-Arakan basin. *Journal of Petroleum Exploration and Production Technology, 9*(1), 297–305.

Tong, M., & Tao, H. (2008). Permeability estimating from complex resistivity measurement of Shaly Sand reservoir. *Geophysical Journal International, 173*(2), 733–739.

Umnova, O., Attenborough, K., Shin, H.-C., & Cummings, A. (2005). Deduction of tortuosity and porosity from acoustic reflection and transmission measurements on thick samples of rigid-porous materials. *Applied Acoustics, 66*(6), 607–624.

Winsauer, W. O., Shearin, A. M., Masson, P. H., & Williams, M. (1952). Resistivities of brine saturated sands in relation to pore geometry. *AAPG Bulletin, 36*(2), 253–277.

Worthington, P. F. (1993). The uses and abuses of the Archie equations, 1: the formation factor-porosity relationship. *Journal of Applied Geophysics, 30*(3), 215–228.

Wyckoff, R. D., Botset, H. G., Muskat, M., & Reed, D. W. (1933). The measurement of permeability of porous media for homogeneous fluids. *Review of Scientific Instruments, 4*(7), 394–405.

Wyllie, M. R. J., & Spangler, M. B. (1952). Application of electrical resistivity measurement to problem of fluid flow in porous media. *AAPG Bulletin, 36*(2), 359–403.

Yu, B.-M., & Li, J.-H. (2004). A geometry model for tortuosity of flow path in porous media. *Chinese Physics Letter, 21*(8), 1569–1571.

Yun, M., Yu, B., Xu, P., & Wu, J. (2006). Geometric models for tortuosity of streamlines in three-dimensional porous media. *Canadian Journal of Chemical Engineering, 84*(3), 301–309.